Ojiro *et al. Robomech J* (2020) 7:24
https://doi.org/10.1186/s40648-020-00173-2

ROBOMECH Journal

RESEARCH ARTICLE Open Access

High precision control model of large-sized gantry-type linear motor slider

Tetsuya Ojiro[1*], Toshiyuki Tachibana[2], Hideki Honda[3], So Watanabe[4], Hiroshi Hamamatsu[5] and Kazuhiro Tsuruta[1]

Abstract

Large-sized gantry-type linear motor sliders are widely used in industry (e.g. in liquid crystal panel production equipment). An appropriate control model is important for deriving control methods to improve control performance. Although various control models of large-sized gantry-type linear motor sliders have been developed in previous studies, no results are yet reported regarding control models which precisely reproduce characteristics of a large-sized gantry-type linear motor slider. In general, a method to derive a transfer function by using frequency responses can be employed to obtain an accurate control model, however, large sized gantry-type linear motor sliders have unique characteristics, namely "distortion" and "coupling", thus the transfer function derived using only the frequency response cannot reproduce the experimental results with high accuracy. In this paper we report on a method to obtain a highly precise control model of a large sized gantry-type linear motor slider.

Keywords: Large-sized gantry-type linear motor slider, Frequency response, Transfer functions modification

Introduction

In recent years, number of applications of linear motors in industry has increased [1, 2]. For example, linear motors are used for carrying thin steel plates in the steel industry [3]. However, to carry heavy loads, the linear motor slider is required to have a sufficient power. When aiming at higher power of a single linear motor, special design and individual manufacturing are required to produce a large-sized motor. Special permanent magnets are used to achieve strong magnetic fields, which with other various issues inevitably contribute to costs [4–6]. Therefore, low-cost gantry type linear motor sliders, which enable high output power, are used. Applications include for example liquid crystal panel production devices [7, 8] or feed drives of machining centers [9].

To improve control performance of a gantry-type linear motor slider, it is important to develop a precise control model. In the previous studies, a control model of large-sized gantry-type linear motor slider was developed by using a spring-mass-damper system [4]. However, all frequency characteristics (e.g. yawing vibration and pitching vibration [10], machine stand vibration [11]) were not considered in the control model, thus the accuracy of the control model was not sufficient. For example, the oscillation phenomenon, which occurs in the actual experimental machine when high feedback gain is applied, is not reproduced with the developed control model. Ref. [10] uses a model that takes pitching and yawing vibrations into consideration. However, in Ref. [10] feedback gain is gradually increased with a goal to the problem each time separately. Therefore, numerous experiments are required to increase feedback gain, which takes time and costs. As a method of deriving a model to be capable of reproducing all frequency responses in a single experiment, a method to derive a transfer function using frequency responses is available. However, large sized gantry-type linear motor sliders have unique characteristics, namely "distortion" and "coupling". Ref. [12] proposes a control model that can reproduce all frequency

*Correspondence: t-ojiro@ip.kyusan-u.ac.jp
[1] Department of Mechanical Engineering, Faculty of Science and Engineering, Kyushu Sangyo University, 2-3-1, Matsukadai, Higashi-ku, Fukuoka 813-8503, Japan
Full list of author information is available at the end of the article

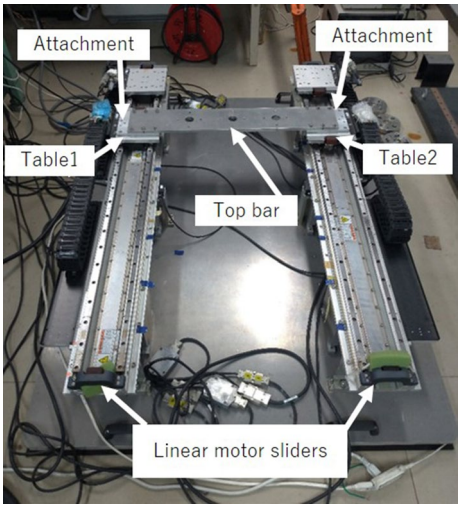

Fig. 1 Gantry-type linear motor slider

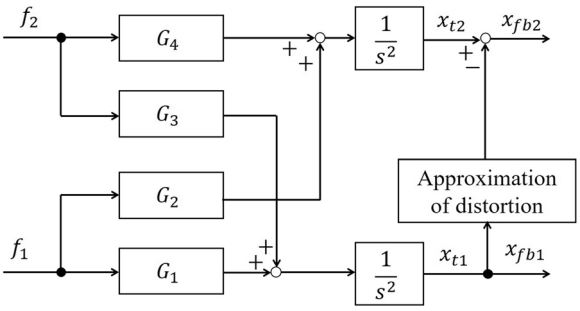

Fig. 2 Identified control model

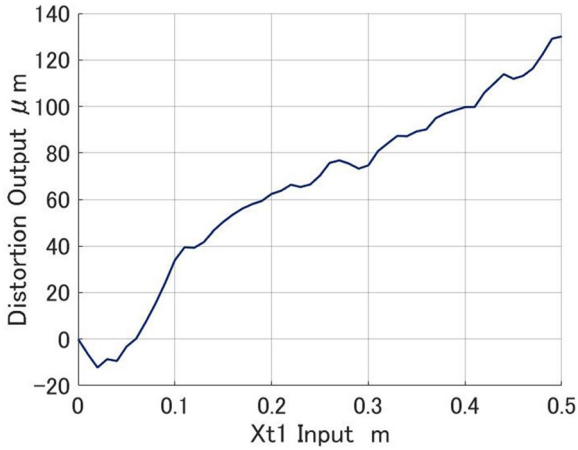

Fig. 3 Distortion of the gantry type linear motor slider

Table 1 Specifications of experimental equipment

Linear slider	SGT1F32-107AH20-0 (YASKAWA)
Linear motor	SGLFW-35A120A (YASKAWA)
Rated force	80 N
Max force	220 N
Table mass	3.9 kg
Base mass	42 kg
Stroke	1070 mm
Distance between two sliders	500 mm

characteristics and unique characteristics of the large sized gantry-type linear motor slider. However, since Ref. [12] does not consider friction, the experimental results cannot be accurately reproduced. In this paper we demonstrate that the experimental results could be accurately reproduced by considering friction.

Methods/experimental

Experimental equipment [12]

Figure 1 shows a large-sized gantry-type linear motor slider which is used in this research. The experimental equipment is comprised of two sliders arranged in parallel and linked by two attachments and a top bar. This experimental equipment has "distortion" and "coupling" which are the problems of large machines [12]. The sliders have linear encoders that measure the position of each table with a resolution of 0.5 μm. Table 1 shows the main specifications of each linear motor slider.

Control model derivation [12]

Figure 2 shows a block diagram of the defined control model. Here f_1 and f_2 are force references to each linear motor slider, $G_1(s)$, $G_2(s)$, $G_3(s)$ and $G_4(s)$ are transfer functions from each force reference to each acceleration, s is Laplace operator, x_{t1} and x_{t2} are positions of two tables, "Approximation of distortion" block is same block used in Ref. [4] and [12] which outputs the measured distortion of Fig. 3, and x_{fb1} and x_{fb2} are positions of each table affected by the distortion.

Identification of transfer functions [12, 13]

By using the measured frequency responses, transfer functions which approximate the measured frequency responses were derived. Vibration of the experimental machine was excited by inputting a white noise signal to each linear motor and an acceleration signal was acquired from accelerometers which were attached to the top bar of the experimental machine [12]. Transfer functions G_i, which correspond to $G_1(s)$, $G_2(s)$, $G_3(s)$ and $G_4(s)$, are defined as described by Eq. (1).

$$G_i(s) = \frac{b_{i2}s^2 + b_{i1}s + b_{i0}}{s^2 + a_{i1}s + a_{i0}} \tag{1}$$

In order to determine coefficients of $G_i(s)$, evaluation functions J_i were defined as described by Eq. (2) for each G_i ($i=1,2,3$ and 4), where j is imaginary unit, f_k [Hz] $=0.5\times k$ are frequency responses of H^i with frequencies f_k, and $w_i(f_k)$ are weight functions, applied to each frequency.

$$J_i = \sum_{k=0}^{400} w_i(f_k)\left|G_i(2\pi j f_k) - H_k^i\right|^2 \tag{2}$$

Since J_i represent the differences of frequency responses between G_i and H^i, the optimal coefficients of G_i were derived by minimizing J_i. In this case, values of the weight functions around 100 Hz were set larger than other weight values because all frequency responses have vibration mode at around 100 Hz. Equation (3) shows the condition of the weight function $w_i(f_k)$.

$$w_i(f_k) = \begin{cases} 100 : 100 \le f_k \le 105 \\ 10 : 70 \le f_k < 100 \text{ or } 105 < f_k \le 120 \\ 1 : 0 < f_k < 70 \text{ or } 120 < f_k \end{cases} \tag{3}$$

Table 2 shows the coefficients of transfer functions which are determined by this method. Figure 4 shows comparison of frequency responses H^i and frequency responses of identified transfer functions G_i. Frequency responses of identified transfer functions G_i does not approximate the low-frequency region, but it can be confirmed that the vibration around 100 Hz existing in the experimental machine is well approximated. Therefore, this paper considers that each transfer function can approximate each frequency response.

Table 2 Coefficients of identified transfer functions

i	1	2	3	4
a_{i1}	151.83	117.84	115.93	138.88
a_{i0}	4.46×10^5	4.29×10^5	4.31×10^5	4.51×10^5
b_{i2}	3.77	−0.159	−0.157	3.79
b_{i1}	475.89	324.79	299.97	468.46
b_{i0}	7.95×10^5	6.25×10^5	6.24×10^5	7.76×10^5

Modification of control model

Since the two tables of the gantry-type linear motor slider are coupled by the top bar and the attachments, the position difference between the two tables does not exceed a certain range. Figure 5 shows the measured position difference when 40 N step force reference was input to one of the linear motor sliders [4]. A difference between (a) and (b) is a difference in input. According to these results, it is verified that position difference between the two tables without distortion converges to a certain value when step force input is applied to one of the linear motor sliders. However, the derived transfer function cannot reproduce this characteristic. Therefore, the transfer function needs to be modified.

In order to reproduce the characteristic caused by coupling of the two tables, the position difference between the two tables should converge to a certain value when

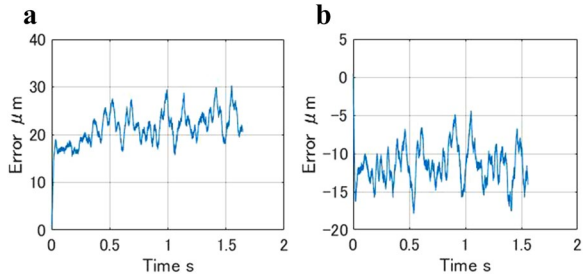

Fig. 5 Measured position difference between two tables. **a** Step force reference input to F_1, **b** Step force reference input to F_2

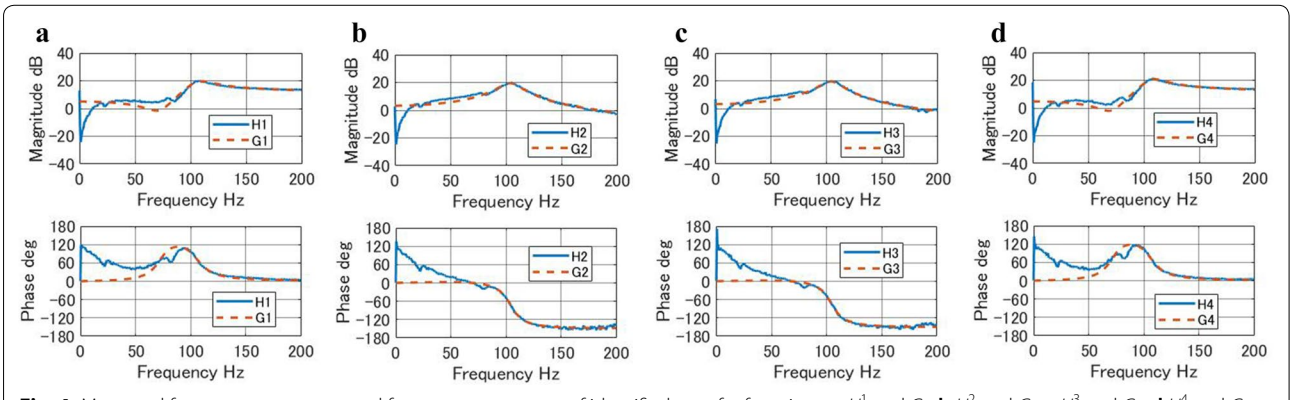

Fig. 4 Measured frequency responses and frequency responses of identified transfer functions. **a** H^1 and G_1, **b** H^2 and G_2, **c** H^3 and G_3, **d** H^4 and G_4

the input step force reference is applied to one of the two sliders in the control model.

According to the final value theorem, the final values of position difference for step force reference can be written as Eqs. (4) and (5). Two responses of the position differences to force reference $f_1(t)$ and $f_2(t)$ were defined as $e_1(t)$ and $e_2(t)$ respectively.

$$\lim_{t\to\infty} e_1(t) = \lim_{s\to 0} sE_1(s) = \lim_{s\to 0} \frac{1}{s^2}(G_1 - G_2) \tag{4}$$

$$\lim_{t\to\infty} e_2(t) = \lim_{s\to 0} sE_2(s) = \lim_{s\to 0} \frac{1}{s^2}(G_3 - G_4) \tag{5}$$

To develop a control model which reproduces the characteristics caused by the tables coupling, Eqs. (4) and (5) should converge. Convergence conditions of these limits can be written as Eqs. (6)–(8) by using coefficients of transfer functions G_i as shown in Eq. (1).

$$a_{20}b_{10} - a_{10}b_{20} = 0 \tag{6}$$

$$a_{20}b_{11} + a_{21}b_{10} - a_{10}b_{21} - a_{11}b_{20} = 0 \tag{7}$$

$$a_{40}b_{30} - a_{30}b_{40} = 0 \tag{8}$$

$$a_{40}b_{31} + a_{41}b_{30} - a_{30}b_{41} - a_{31}b_{40} = 0 \tag{9}$$

To satisfy these equations, coefficients of transfer functions in the control model were modified. In this case, not to change the frequency characteristics of the resonance point, poles of each transfer function should not be changed. Therefore, the coefficients of numerator of transfer function, b_{11}, b_{20}, b_{30}, and b_{41} were replaced by b'_{11}, b'_{20}, b'_{30} and b'_{41} as shown in Eqs. (10) to (13) respectively.

$$b'_{20} = \frac{a_{20}b_{10}}{a_{10}} \tag{10}$$

$$b'_{30} = \frac{a_{30}b_{40}}{a_{40}} \tag{11}$$

$$b'_{11} = \frac{1}{a_{20}}\left(a_{10}b_{21} + a_{11}b'_{20} - a_{21}b_{10}\right) \tag{12}$$

$$b'_{41} = \frac{1}{a_{30}}\left(a_{40}b_{31} + a_{41}b'_{30} - a_{31}b_{40}\right) \tag{13}$$

Then the modified transfer functions were defined as $G'_1(s)$, $G'_2(s)$, $G'_3(s)$ and $G'_4(s)$. Table 3 shows the coefficients of each modified transfer function. For the following discussion, the control model using $G'_1(s)$, $G'_2(s)$, $G'_3(s)$ and $G'_4(s)$ instead of $G_1(s)$, $G_2(s)$, $G_3(s)$ and $G_4(s)$ is defined as a modified control model.

Table 3 Coefficients of modified transfer functions

i	1	2	3	4
a_{i1}	151.83	117.84	115.93	138.88
a_{i0}	4.46×10^5	4.29×10^5	4.31×10^5	4.51×10^5
b_{i2}	3.77	−0.159	−0.157	3.79
b_{i1}	389.89	324.79	299.97	344.46
b_{i0}	7.95×10^5	7.65×10^5	7.42×10^5	7.76×10^5

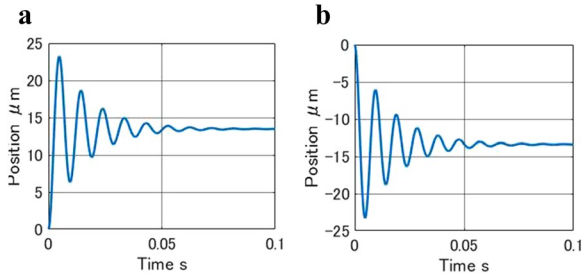

Fig. 6 Responses of $e'_1(t)$ and $e'_2(t)$ for step force reference. **a** Response of $e'_1(t)$, **b** Response of $e'_2(t)$

In the modified control model, responses of position difference for force references $f_1(t)$ and $f_2(t)$ were defined as $e'_1(t)$ and $e'_2(t)$ respectively.

Figure 6 shows the responses $e'_1(t)$ and $e'_2(t)$ for 40 N step force reference. It can be confirmed that both step responses converge to a certain value. Additionally, in comparison with results of actual experiment, shown in Fig. 5, convergence value is relatively close.

Figure 7 shows comparison between measured frequency response, frequency response of identified transfer function, and frequency response of modified transfer function. It can be seen that influence on frequency response by the coefficients modifications is small enough for all frequency responses and each G'_i well approximates the measured frequency response.

Therefore, it can be said that modified control model which reproduces the characteristics of coupled tables was derived without changing frequency characteristics of the identified control model.

Results and discussion

Verification of simulation model

In order to verify the validity of the modified control model, comparison between the simulation results of modified control model and actual experimental results was conducted. In the previous research, the results of control experiments which used the same experimental

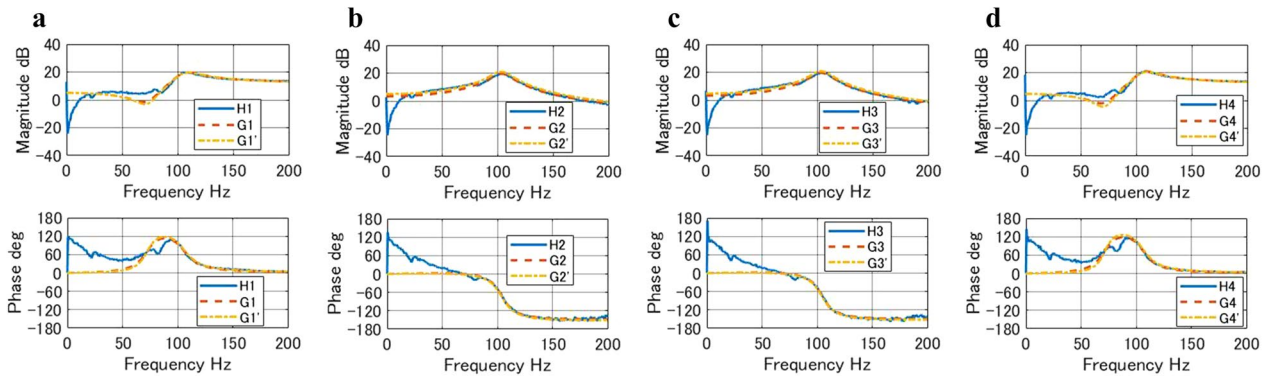

Fig. 7 Comparison of measured frequency responses H^i and transfer functions G_i and G'_i. **a** H^1, G_1 and G'_1, **b** H^2, G_2 and G'_2, **c** H^3, G_3 and G'_3, **d** H^4, G_4 and G'_4

Table 4 Parameters of friction

n	1	2
F_{sn}	14.78 N	16.43 N
v_{sn}	0.04 m/s	0.03 m/s
a_n	−6.67	−7.42
F_{vn}	34.09 N/(m/s)	36.68 N/(m/s)
F_{cn}	9.92 N	12.16 N

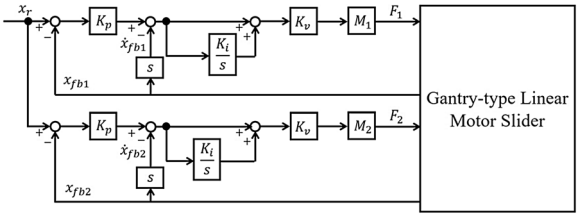

Fig. 8 Block diagram of Control method 1

equipment as in this research were reported. In Ref. [4], P-PI control for each axis was applied for the control experiment and the results show that reaction force occurred between the two tables. In Ref. [14], a control method that suppresses reaction force was applied and the results show that the reaction force was suppressed with low feedback loop gain. However, with high feedback loop gain, vibration of force reference occurred.

In this research, control simulations were conducted with these two control methods and it was verified that the same phenomenon occurs in the simulations. The simulations were implemented by using MATLAB/Simulink programs.

Furthermore, the experimental machine of this study is the same as the experimental machine of Ref. [4], therefore, the same friction model is used as in Ref. [4]. Equation (14) shows the friction model and the Table 4 shows the parameters of friction.

$$F_{dn} = \begin{cases} F_n : \text{if} |F_n| \le F_{sn} \text{ at } v_{tn} = 0 \\ \text{sgn}(v_{tn}) F_{sn} e^{-|v_{tn}| a_n} : 0 < |v_{tn}| \le v_{sn} \\ v_{tn} F_{vn} + \text{sgn}(v_{tn}) F_{cn} : v_{sn} < |v_{tn}| \end{cases} \quad (14)$$
$$(\text{n} = 1 \text{ or } 2)$$

Here F_{dn} is friction disturbance, F_{sn} is maximum static friction force, v_{tn} is table velocity, a is power index to express friction characteristic in a region below Stribeck velocity, v_{sn} is Stribeck velocity, F_{vn} is viscous friction coefficient, and F_{cn} is Coulomb friction.

Simulation with control method 1 [4]

As the control method 1, proportional-position-proportional-integral-velocity (P-PI) control for each axis, as shown in Ref. [4] was used. Therefore, the force references for each axis are shown in Eqs. (15) and (16). Figure 8 shows block diagram of control method 1.

$$F_1 = M_1 \left[K_v \{ K_p (x_r - x_{fb1}) - \dot{x}_{fb1} \} + K_i \int K_v \{ K_p (x_r - x_{fb1}) - \dot{x}_{fb1} \} dt \right] \quad (15)$$

$$F_2 = M_2 \left[K_v \{ K_p (x_r - x_{fb2}) - \dot{x}_{fb2} \} + K_i \int K_v \{ K_p (x_r - x_{fb2}) - \dot{x}_{fb2} \} dt \right] \quad (16)$$

where M_1 and M_2 are nominal masses of each table, x_{fb1} and x_{fb2} are position responses of each table, K_p is position proportional gain, K_i is velocity integral gain, K_v is

Table 5 Feedback loop gain for control method 1

	K_p	K_v	K_i
Case 1-1	25 1/s	100 1/s	100 1/s
Case 1-2	50 1/s	200 1/s	200 1/s

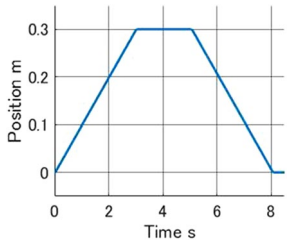

Fig. 9 Position reference

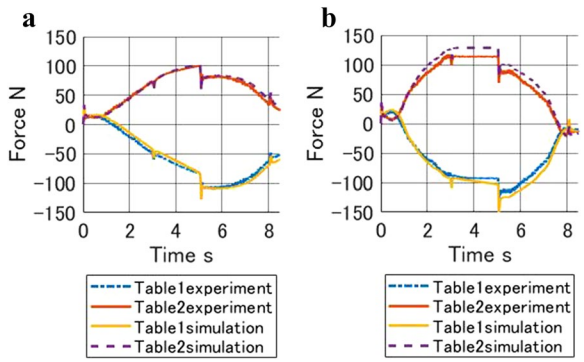

Fig. 10 Results of simulation and comparison with experimental results in control method 1. **a** Case1-1, **b** Case1-2

velocity proportional gain, and x_r is position reference, s is Laplacian operator.

In this simulation, position reference and feedback loop gain are set to the same values as in Ref. [4]. The conditions of feedback loop gain are shown in Table 5 and position reference is shown in Fig. 9.

Figure 10 shows results of the simulation and comparison with the experimental results. Figure 10 shows that reaction forces between Tables 1 and 2 occurred also in the simulation. Simulation result has the same characteristics of experimental result. Therefore, under the conditions of control method 1, the control model approximates the actual experimental results.

Simulation with control method 2 [10, 14]

As the control method 2, a method that suppresses the reaction force, which is shown in Ref. [14] was used. Therefore, force references for each linear motor are shown in Eqs. (17) and (18), where l is distance between

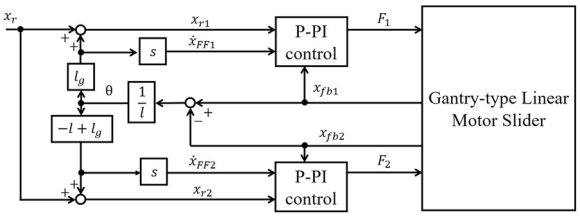

Fig. 11 Block diagram of Control method 2

Table 6 Feedback loop gain for control method 2

	K_p	K_v	K_i
Case 2-1	100 1/s	400 1/s	400 1/s
Case 2-2	125 1/s	500 1/s	500 1/s

Tables 1 and 2, l_g is distance between Table 1 and center of the mass, and θ is rotation angle. Other parameters have the same meaning as in control method 1. Control method 2 is based on the P-PI control. Hence, it considers θ but has no control over it, paying closer attention to the work-point position on the top bar of the linear motor slider, which in general is the center-of-mass of the top bar. Figure 11 shows block diagram of control method 2.

$$F_1 = M_1\left[K_v\{K_p(x_{r1}-x_{fb1})-\dot{x}_{fb1}+\dot{x}_{FF1}\} + K_i\int K_v\{K_p(x_{r1}-x_{fb1})-\dot{x}_{fb1}+\dot{x}_{FF1}\}dt\right] \tag{17}$$

$$F_2 = M_2\left[K_v\{K_p(x_{r2}-x_{fb2})-\dot{x}_{fb2}+\dot{x}_{FF2}\} + K_i\int K_v\{K_p(x_{r2}-x_{fb2})-\dot{x}_{fb2}+\dot{x}_{FF2}\}dt\right] \tag{18}$$

where

$$x_{r1} = x_r + l_g\theta \tag{19}$$

$$x_{r2} = x_r - (l-l_g)\theta \tag{20}$$

$$\dot{x}_{FF1} = l_g\dot{\theta} \tag{21}$$

$$\dot{x}_{FF2} = -(l-l_g)\dot{\theta} \tag{22}$$

$$\theta = \frac{x_{fb1}-x_{fb2}}{l} \tag{23}$$

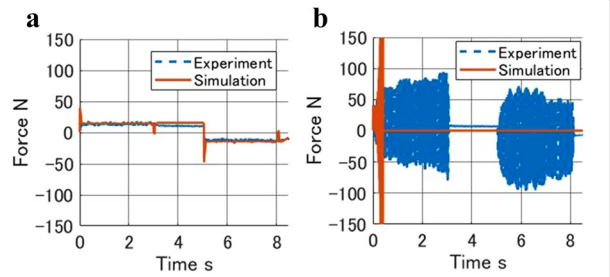

Fig. 12 Results of simulation and comparison with experimental results in control method 2. **a** Case2-1, **b** Case 2-2

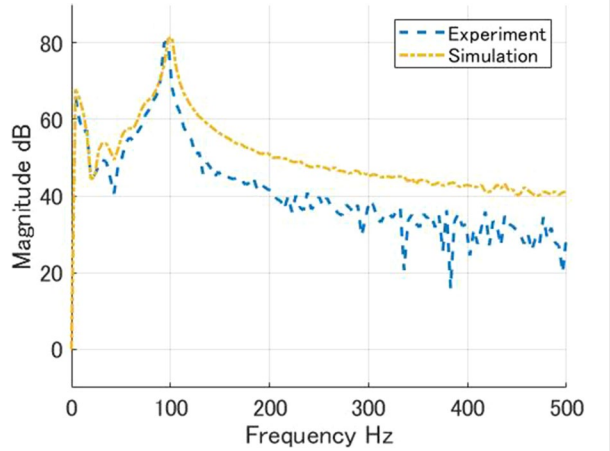

Fig. 13 Amplitude spectrum of force reference F_1 in Case 2-2

The conditions of feedback loop gain are shown in Table 6 and position reference is shown in Fig. 9. In this simulation, if the force reference exceeds 500 N, the simulation stops automatically. Figure 12 shows the results of the simulation and comparison with the experimental results. In Fig. 12, only F_1 is shown as a force reference because F_1 and F_2 are exactly the same. In case 2-1, in both simulation and experiment, the reaction forces between the two tables were suppressed. Moreover, the force reference is substantially the same as the experimental result. In case 2-2, the force reference vibrates. In the simulation, the force reference diverged rapidly, and the simulation stopped because magnitude of the force reference exceeded 500 N. However, in the actual experiment, the force reference vibrated within the range of ± 100 N. To analyze the characteristics of force reference vibration, Fast-Fourier-Transformation was applied, and amplitude spectrum was acquired. Figure 13 shows amplitude spectrum of force reference F_1 in case 2-2. According to the amplitude spectrum, it can be seen that each force reference vibrates at the same frequency of 100 Hz. Additionally, based on the position response, a velocity response of actual experiment was calculated by using Euler approximation. Figure 14 shows velocity response in the simulation and in the actual experiment. Figure 14b, d can be seen that vibrations of V_{fb1} and V_{fb2} are in phase. Therefore, the signal values in Figs. 12 and 14 are different between the experimental results and the simulation results. However, experimental results and simulation results have the same tendency. In Case 1, the slider operates safely, but in Case 2, vibration occurs. In every condition of feedback loop gain, all simulation results in control method 2 are similar to the experimental results.

Conclusion

In this research, highly precise control model that can reproduce all frequency characteristics and unique characteristics of a large-sized gantry-type linear motor slider was derived. According to comparison of simulations and actual experiments which were implemented with two control methods, the control model well approximates characteristics of a gantry-type linear motor slider. A control method for improving the control performance of large-sized gantry-type linear motor slider can be derived by using this model. Future study topic is verification of

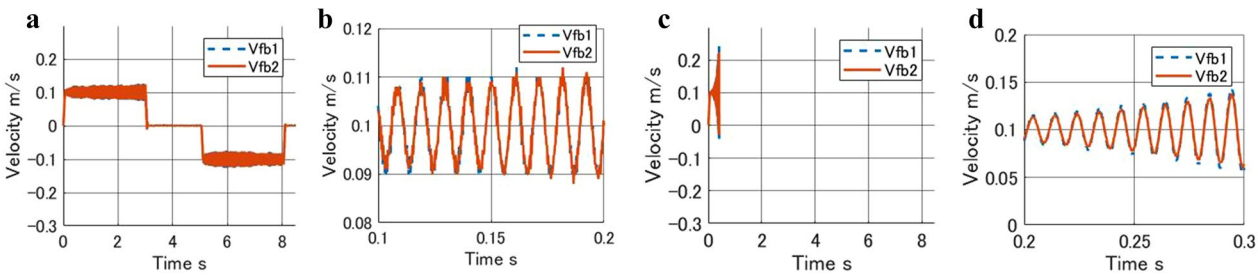

Fig. 14 Comparison of velocity response of simulation and actual experiment in Case 2-2. **a** Velocity response of actual machine, **b** velocity response of actual machine (enlarged), **c** velocity response of simulation, **d** velocity response of simulation (enlarged)

validity of the proposed method when characteristics of actual machine change, for example, the movement of the center of gravity in real time.

Acknowledgements
Not applicable.

Authors' contributions
TO and TT developed the system and carried out the experiments and simulations. HHo, SW and KT managed the study. HHa managed the experiments. All members verified the content of their contributions. All authors read and approved the final manuscript.

Funding
Not applicable.

Availability of data and materials
The datasets used and/or analyzed in this study are available from the corresponding author on request.

Competing interests
The authors declare that they have no competing interests.

Author details
[1] Department of Mechanical Engineering, Faculty of Science and Engineering, Kyushu Sangyo University, 2-3-1, Matsukadai, Higashi-ku, Fukuoka 813-8503, Japan. [2] Research Institute of Systems Planning, Inc., 18-6 Japan Hall, Sakuragaokacho, Shibuya-ku, Tokyo 150-0031, Japan. [3] Department of Biological Functions Engineering, Graduate School of Life Science and Systems Engineering, Kyushu Institute of Technology, 2-4, Hibikino, Wakamatsu-ku, Kitakyushu 808-0196, Japan. [4] Department of Mechanical Engineering, National Institute of Technology, Kagoshima College, 1460-1 Shinko, Hayato-cho, Kirishima 899-5193, Japan. [5] Department of Creative Engineering, National Institute of Technology, Kitakyushu College, 5-20-1 Shii, Kokuraminami-ku, Kitakyushu 802-0985, Japan.

Received: 19 December 2019 Accepted: 23 May 2020
Published online: 28 May 2020

References

1. Haidong Y, Babak F (2010) Industrial servo applications of linear induction motors based on dynamic maximum force control. In: 2010 twenty-fifth annual IEEE applied power electronics conference and exposition (APEC), Palm Springs, CA, 21–25 Feb; 2010
2. Nakamura Y, Morimoto K, Wakui S (2011) Position control of linear slider via feedback error learning. In: 2011 third pacific-asia conference on circuits, communications and system (PACCS), Wuhan, China, 17–18 July 2011
3. Yamada T, Fujisaki K (2009) Application of linear induction motor for tension supply and heating to thin sheet steel. Electr Eng Jpn 168(2):38–47
4. Ojiro T, Honda H, Tsuruta K, Hanamoto T (2018) Control model for large-sized gantry type linear motor slider. Electr Eng Jpn 203(2):39–46
5. Nakashima R, Hao S, Honda H, Oguro R, Miyakawa H, Tsuji T (2003) Position control for a linear slider with twin linear drives. Electr Eng Jpn 147(4):68–76
6. Sato K, Tsuruta K, Kikuchi T, Honda H (2008) A robust adaptive control for parallel linear sliders using decoupling model. In: 2008 SICE annual conference, Tokyo, Japan, 20–22 Aug; 2008
7. Terasaki F, Kobayashi J, Oguro R, Ohkawa F (2006) A positioning control of a serial twin linear slider system with machine stand vibration. In: 2006 IEEE international conference on industrial technology, Mumbai, India 15–17 Dec. 2006
8. Tomita Y, Kojima E, Kawachi S, Koyanagawa Y, Ootsuka S (2012) Development and applications of sumitomo precision stage technologies for FPD process. J Jpn Soc Precis Eng 78(2):117–121
9. Sogabe M, Iwashita Y, Sonoda N, Kakino Y (2007) A study on the servo-stability of the tandem driven machine with linear motors. J Jpn Soc Precis Eng 73(5):605–610
10. Ojiro T, Tachibana T, Honda H, Hamamatsu H, Tsuruta K, Hanamoto T (2019) Consideration of multi-degree of freedom vibration on large-sized gantry type linear motor slider. J Robot Mechatr JRM 31(2):240–250
11. Watanabe S, Oguro R, Kobayashi J, Ohkawa F (2006) A decoupling method for serial twin linear slider system with machine stand vibration. Proc IEEE Int Symp Ind Electron 2006:3032–3037
12. Tachibana T, Ojiro T, Hamamatsu H, and Honda H(2019) Study on Control Model Structuring of Large-Sized Gantry-Type Linear Motor Slider by Measuring Frequency Response. The 5th IEEJ international workshop on Sensing, Actuation, Motion Control, and Optimization (SAMCON2019) TT2-2
13. Levy EC (1959) Complex-curve fitting. In: IRE transaction on automatic control. AC-4. pp 37–44
14. Ojiro T, Honda H, Hanamoto T, Tsuruta K (2017) Consideration on control method of the large-sized gantry-type linear motor slider. In: 2017 IEEE international conference on mechatronics and automation (ICMA). pp 1198–1203

Publisher's Note